Coherent structures detection within a dense Alpine forest

I.M. Cely-Toro [a], L. Mortarini [a,b,*], C.Q. Dias-Júnior [c], U. Giostra [d], L. Buligon [a], G.A. Degrazia [a], D. Cava [b]

[a] *Universidade Federal de Santa Maria, Santa Maria (RS), Brazil*
[b] *National Research Council, Institute of Atmospheric Sciences and Climate, Italy*
[c] *Federal Institute of Pará, Department of Physics, Belém, Brazil*
[d] *Università degli Studi di Urbino Carlo Bo, Department of Pure and Applied Sciences (DiSPeA), Urbino, Italy*

ARTICLE INFO

ABSTRACT

The influence of coherent vortices on the turbulence structure above and below a dense plant canopy is investigated using turbulence measurements collected at five levels on top and inside a coniferous forest on an Alpine Plateau. Five different stability regimes, from free convection to very stable stratification, were identified and considered in the analysis. Coherent structures are detected by fitting the vertical velocity auto-correlation functions with a theoretical oscillating function. This allowed to evaluate the coherent vortices characteristic timescales and to discriminate between turbulent data subsets characterized by fine-scale turbulence and subsets in which turbulence is dominated by coherent structures generated at the canopy top. An original methodology to fit cross-correlation function and to single out the most energetic frequency in presence of periodic behaviour is presented and applied to the turbulent momentum flux. The analysis shows how not far from neutral conditions the dominant time scale of the momentum flux is mainly determined by the longitudinal wind velocity component, rather than vertical one, while in free convection and very stable conditions coherent vortices do not seem to influence the momentum transport, dominated by large-scale structures. This is confirmed by the fine-scale turbulence and coherent structures efficiency in turbulence transport throughout the stability regimes.

1. Introduction

In recent years, experimental (Gao et al., 1989; Paw U et al., 1992; Chen et al., 1997; Dupont and Patton, 2012b,a; Cava et al., 2022; Mortarini et al., 2022), theoretical (Raupach et al., 1996; Finnigan et al., 2009) and numerical studies (Su et al., 1998; Foster et al., 2006; Drobinski et al., 2007; Dias-Júnior et al., 2015) highlighted the important role of coherent structures (CS) on the flow dynamics within and above plant canopies. The literature refers to 'coherent structures' as three-dimensional, well-organized flow patterns with characteristic forms and timescale in which fundamental flow variables (such as wind velocity or temperature) exhibit significant correlation with themselves and with each other in a range of space and time that are significantly larger than the high-frequency turbulent scales (Robinson, 1991; Serafimovich et al., 2011). CS in a roughness sublayer (RSL, i.e. the portion of the atmosphere dynamically influenced by the canopy structure, typically extending up to 2–3 times the mean canopy height, h) are organized in cycles of ejections (weak rising motions) and sweeps (energetic and intermittent downward gusts) and may be revealed by periodic ramp and triangle-like patterns in scalar and vector time series, respectively (Gao et al., 1989; Raupach et al., 1989; Paw U et al., 1992; Dwyer et al., 1997; Finnigan, 2000; Thomas and Foken, 2007; Katul et al., 2013). Ramp patterns in scalar time series were primarily observed within and above high plant canopies by Bergström and Högström (1989) and Gao et al. (1989). They showed that distinct ejection/sweep cycles can act on a scalar gradient to produce 'micro-fronts' and highlighted their important role in the exchange processes between forest and atmosphere. Comparison of various experiments revealed that flux contributions from CS in the RSL may range from 40% to 90% of the total flux for periods of 1 to 2 h (Barthlott et al., 2007). CS produce higher turbulent diffusivities in the RSL and may be able to couple the layers above and within the canopy, simultaneously affecting large vertical extents and producing counter-gradient fluxes often observed in the RSL (Brunet, 2020).

In the literature various techniques for detecting CS in wind velocity components and scalar time series were developed. Preliminary methods were based on the visual identification of ramps in scalar time series

and, hence, could be easily applied only to limited data sets (Gao et al., 1989). Conditional sampling approaches to extract strong fluctuations from the temporal mean or to identify ejection/sweep patterns through quadrant analysis proved to be a more promising approach (Antonia, 1981; Raupach and Thom, 1981; Bergström and Högström, 1989; Gao et al., 1989). However, even if capable of quantifying the CS contribution to fluxes, quadrant analysis is unable to characterize such structures in terms of spatial scale and temporal evolution (Thomas and Foken, 2005). The wavelet transform (Farge, 1992; Daubechies, 1992) represented a powerful tool for implementing automated detection algorithms easily applicable to large datasets and able to identify the CS and their contribution to fluxes over and within forests and other roughness elements (Collineau and Brunet, 1993a,b; Feigenwinter and Vogt, 2005; Thomas and Foken, 2005, 2007; Barthlott et al., 2007; Serafimovich et al., 2011; Dias-Júnior et al., 2017). Wavelets provide multi-resolution analysis, that simultaneously captures time and frequency information and detects isolated events providing information about their time of occurrences and characteristics. Wavelet-based detection schemes are optimal for studying intermittent or transient processes; however, interpreting the complex two-dimensional signal produced by the wavelet transform can be a difficult and meticulous task. Even for a turbulent velocity time-series with no CS, the wavelet transform identifies multiple energy peaks, which are difficult to interpret (Dunyak et al., 1998). In presence of CS and concurrent mechanisms (like horizontal meandering in strong stability or convective structures in free convection) the wavelet signal analysis can be even more delicate. Recently, a methodology based on the Eulerian Autocorrelation Function (EAF), originally developed for detecting large-scale submeso motions (Anfossi et al., 2005; Mortarini et al., 2019) was applied to identify CS at the top of a dense Amazonian forest (Mortarini et al., 2022). CS were identified through a non-linear fit of the 5 min autocorrelation function of the turbulent variables with a decaying, oscillating exponential function. The oscillating frequency of the fitting function was linked to the most energetic frequency in the spectrum and consequently to the characteristic temporal scale of the coherent vortices. The application of this new methodology allowed to investigate and parameterize the behaviour of the time and separation length scales of CS in different stability regimes as a function of the shear length scale close to the canopy top.

The presence of CS strongly affects the RSL and, as a consequence, the traditional law-of-the-wall or the standard Monin–Obukhov Similarity Theory (MOST) flux-gradient relationships, often used in meteorological or climate models to predict vertical turbulent fluxes at the surface, fail in the RSL requiring the introduction of appropriate corrections (Harman and Finnigan, 2007, 2008; Chor et al., 2017; Mortarini et al., 2023). Hence, a careful understanding of coherent motion dynamics is essential for a truthful description of the turbulent dispersion above vegetated surfaces. The characteristics of coherent motions were theoretically explained through the plane mixing-layer analogy, that have led to significant improvement in modelling the flow in the RSL (Raupach et al., 1996; Harman and Finnigan, 2007, 2008). According to the mixing-layer analogy, CS evolve from Kelvin–Helmholtz instabilities triggered by the wind shear at the top of the vegetation; their vertical scale (L_s, the 'canopy-shear length scale') is proportional to the vorticity thickness related to the inflection point of the wind velocity profile (Raupach et al., 1996). The applicability of the mixing-layer analogy has been assessed for neutral conditions or, anyway, for thermal conditions close to neutrality (Shaw et al., 1995; Brunet and Irvine, 2000; Dupont and Patton, 2012a; Patton et al., 2016), whereas it has been shown that other mechanisms may influence the flow dynamics in convective conditions and strong stable stratification (Cava et al., 2022). In unstable conditions, the organization of turbulence in the RSL is a combination of CS generated by shear processes and larger convective eddies. As atmospheric instability increases, the inflection in the wind velocity profile progressively weakens (Dias-Júnior et al., 2013) leading to a domination of RSL

flow by warm updrafts (canopy plumes) and cool downdrafts in free convection limit (Villani et al., 2003; Thomas et al., 2006; Dupont and Patton, 2012a; Patton et al., 2016). In stable conditions, CS are damped by buoyancy as stability increases; observational studies showed that they tend to become highly intermittent and unable to penetrate in the deeper layers of the vegetation (Launiainen et al., 2007; Dupont and Patton, 2012a,b), similar results were found from DNS analyses (Ansorge and Mellado, 2014, 2016; Allouche et al., 2022). In very stable conditions, CS remain confined close to the canopy top (Cava et al., 2022) or may resemble waves ('canopy waves') with similar time scale, transporting energy but not mass (Lee and Baar, 1998; Cava et al., 2004). Further, the flow characteristics may be strongly influenced by the presence of large-scale submeso motions (Mortarini et al., 2019), such as horizontal meandering or gravity waves, in particular in very stable and low wind regimes. Cava et al. (2022) analysed data collected above and within a dense Amazonian forest, and showed that the increasing atmospheric stratification produced a gradual lowering of the RSL and the consequent propagation of submeso motions up to the canopy top and within the forest, where submeso motions were able to modulate the forest exchange, particularly the scalar fluxes, as already observed by Santos et al. (2016) and Oliveira et al. (2018).

In this work, the influence of CS on the turbulent statistics of the atmospheric flow at the top and within a coniferous forest on an Alpine Plateau was investigated. For this purpose, the EAF methodology used in Mortarini et al. (2022) was extended to study the behaviour of the cross-correlation function between horizontal (u) and vertical (w) wind velocity components and its relationship with the w autocorrelation function. This original approach allowed the detection of CS, as well as the characterization of their temporal scales and the influence on vertical spectrum and momentum cospectral features. Data were conditioned using the EAF methodology for w and the new methodology for uw, separating data sets in classes dominated or not by the presence of CS. The application of the conditioning method at the top of the forest and in the crown region permitted the study of the coupling of the canopy flow at different levels. Also, the ensemble averages of w spectrum and uw co-spectrum in the detected flow classes allowed the investigation of the spectral characteristics and the transport efficiency of different flow structures as a function of the atmospheric stratification.

A brief description of the experimental site is given in Section 2. The proposed methodology for the detection of CS oscillations based on the fit of autocorrelation (ACF) and cross-correlation (CCF) functions and the main results of its application to the experimental data set are described in Sections 3 and 4, respectively.

2. Experimental site

The experimental site, part of a long-term CO_2 flux monitoring program known as CarboEuroflux (Valentini et al., 2000), is an uneven-aged mixed coniferous forest located on an Alpine plateau in Lavarone, Italy (45.96° N, 11.28° E; 1300 masl). The forest is primarily composed of Abies alba (70%), Fagus sylvatica (15%), and Picea abies (15%). It is about 28 m tall (= h) and the tree crown extends up to 10–12 m above the forest floor. The maximum leaf area index (LAI) is 9.6 m^2 m^{-2}, when expressed as half of the total leaf surface area per unit ground area (Chen and Black, 1992), and more than 90% of this leaf area is concentrated in the crown region. The analysed data set were collected as part of a summertime intensive measurement campaign performed between August 09 and October 07, 2000. The micrometeorological tower was placed on a gently rolling plateau and was surrounded by homogeneous vegetation for radial distances exceeding 1 km (Fig. 1). It was equipped with five sonic anemometers situated at 33, 25, 17.5, 11 and 4 m from the forest floor. The turbulent wind velocity components and sonic anemometer temperature were sampled at 20 Hz for the highest and lowest levels by Gill R3 ultrasonic anemometers (Gill Instrument, Lymington, U.K.), whereas at the remaining levels, data
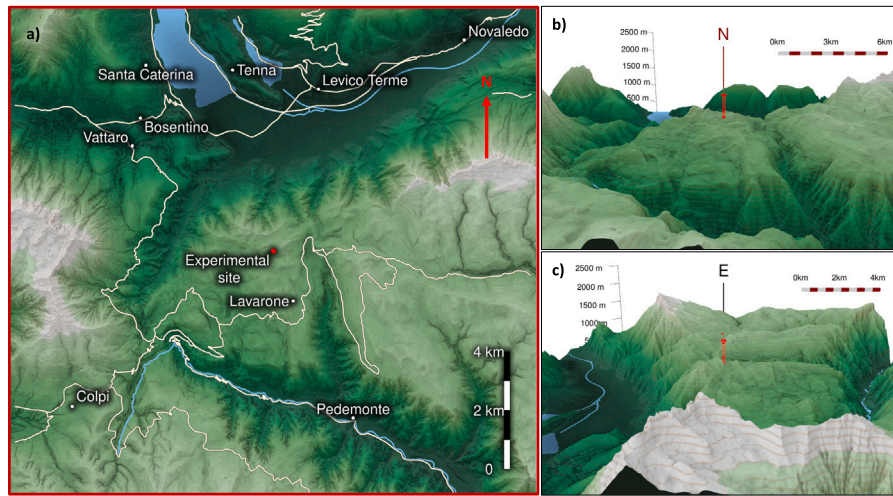
Fig. 1. Map of the region around the Lavarone experimental site (a) and lateral views from S (b) and from W (c).

were sampled at 20.8 Hz using Gill R2 ultrasonic anemometers (Gill Instrument, Lymington, U.K.). Further details on the experimental set-up can be found in Marcolla et al. (2003), Cava et al. (2006) and Cava and Katul (2008).

3. Detection of coherent structure oscillations by correlation function methodology

The periodic behaviour of CS above and below the canopy reflects itself in oscillatory autocorrelation functions. Mortarini et al. (2022) identified the characteristic time scales of CS by fitting 5-min EAFs with a damped oscillating function. In presence of CS, all the wind velocity components and the air temperature autocorrelation functions presented an oscillatory behaviour with different time scales. In this work, Mortarini et al. (2022) approach is extended to study the behaviour of the cross-correlation function between u and w, $C_{uw}(\tau)$, and its relationship with the w autocorrelation function, $R_w(\tau)$. For this purpose, the following functions are considered:

$$R_\chi(\tau) = e^{-p_\chi \tau} \cos(q_\chi \tau); \quad \chi = u, w \tag{1}$$

$$C_{uw}(\tau) = e^{-p_{uw}\tau} \left(\frac{\overline{u'w'}}{\sigma_u \sigma_w} \cos(q_{uw}\tau) + \frac{c}{q} \sin(q_{uw}\tau) \right) \tag{2}$$

in which p_χ and p_{uw} are the inverse of the decorrelation timescales and q_χ and q_{uw} represent the frequencies of oscillation of the auto and cross-correlation functions, respectively; c is a frequency that adjusts the behaviour of the correlation functions near the origin; σ_u and σ_w are standard deviations of horizontal and vertical turbulent wind components, respectively. Fig. 2 shows a 5 min time series of the vertical wind component, w (panel a) and of the instantaneous momentum flux (product of the turbulent fluctuations of the streamwise and the vertical wind components), $u'w'$ (panel b) measured at 33 m in neutral conditions. In panels c and e, the auto and the cross-correlation functions together with their fits represented by Eqs. (1) and (2), respectively, are shown. The evident good comparison with the proposed theoretical behaviour and the experimental results can be further assessed estimating the spectra associated with Eqs. (1) and (2).

Applying a Fourier transform to Eq. (1) the corresponding spectrum can be evaluated:

$$F_\chi(f) = \frac{E_\chi(f)}{\sigma_\chi^2} =$$

$$= \int_0^\infty R_\chi(\tau) \cos(2\pi f \tau) d\tau =$$

$$= 2p_\chi \left(\frac{1}{p_\chi^2 + (q_\chi + 2\pi f)^2} + \frac{1}{p_\chi^2 + (q_\chi - 2\pi f)^2} \right) \tag{3}$$

The cospectrum, i.e. the real part of the cross-spectrum, corresponding to Eq. (2) is the Fourier transform of the even part of C_{uw} (Kaimal and Finnigan, 1994, pp. 60–61):

$$CoF_{uw}(f) = \frac{CoS_{uw}(f)}{\overline{u'w'}} =$$

$$= \int_0^\infty \left[e^{-p_{uw}\,\tau} \cos(q_{uw}\tau) \right] \cos(2\pi f \tau) =$$

$$= 2p_{uw} \left(\frac{1}{p_{uw}^2 + (q_{uw} + 2\pi f)^2} + \frac{1}{p_{uw}^2 + (q_{uw} - 2\pi f)^2} \right) \tag{4}$$

Hence, $F_\chi(f)$ and $CoF_{uw}(f)$ have the same mathematical expression, which cannot represent an Eulerian spectrum (cospectrum), since it does not follow a $-\frac{5}{3}$ ($-\frac{7}{3}$) slope at high frequency. However, they provide an analytical expression for the frequency, f_{peak}, associated to their maximum value. $T_{peak} = f_{peak}^{-1}$ represents the characteristic time scale associated with CS. As a matter of fact, Eqs. (3) and (4) admit a maximum at

$$f_{peak_\Psi} = \frac{1}{2\pi} \sqrt{2\sqrt{q_\Psi^2 \left(p_\Psi^2 + q_\Psi^2\right)} - p_\Psi^2 - q_\Psi^2} \tag{5}$$

with $\Psi = u$, w, uw. Eq. (5) implies that both $F_\chi(f)$ and $CoF_{uw}(f)$ have a maximum only when $m_\Psi = \frac{q_\Psi}{p_\Psi} > \frac{1}{\sqrt{3}}$.

Fig. 3 highlights the role of the m_Ψ parameter in shaping the spectrum and cospectrum behaviours. In particular, for $m_\Psi < \frac{1}{\sqrt{3}}$ the spectrum (or cospectrum) manifests a swift transition between the regime f^0 and the regime f^{-2} (Fig. 3a, black line), looking qualitatively very similar to the spectrum of a non-oscillating function. When $m_\Psi > 1$ the spectrum maximum and, hence, its contribution to the variance of the turbulent variable are more evident (Fig. 3a, red line). Further, the vertical lines identify the spectra and cospectra maxima.

Fig. 2 shows the experimental spectra, $S_w(f)$, (panel d) and the cospectra, $CoS_{uw}(f)$, (panel f), corresponding to the time series depicted in panels a and b. The vertical dashed lines refer to Eq. (5), featuring the ability of the fitting procedure in identifying the more energetic frequency of the spectra.

4. Application of the correlation methodology to experimental data

The methodology proposed in Section 3 was applied to the Lavarone data set in order to detect and characterize CS above and inside the forest in different atmospheric stability conditions. As a preliminary
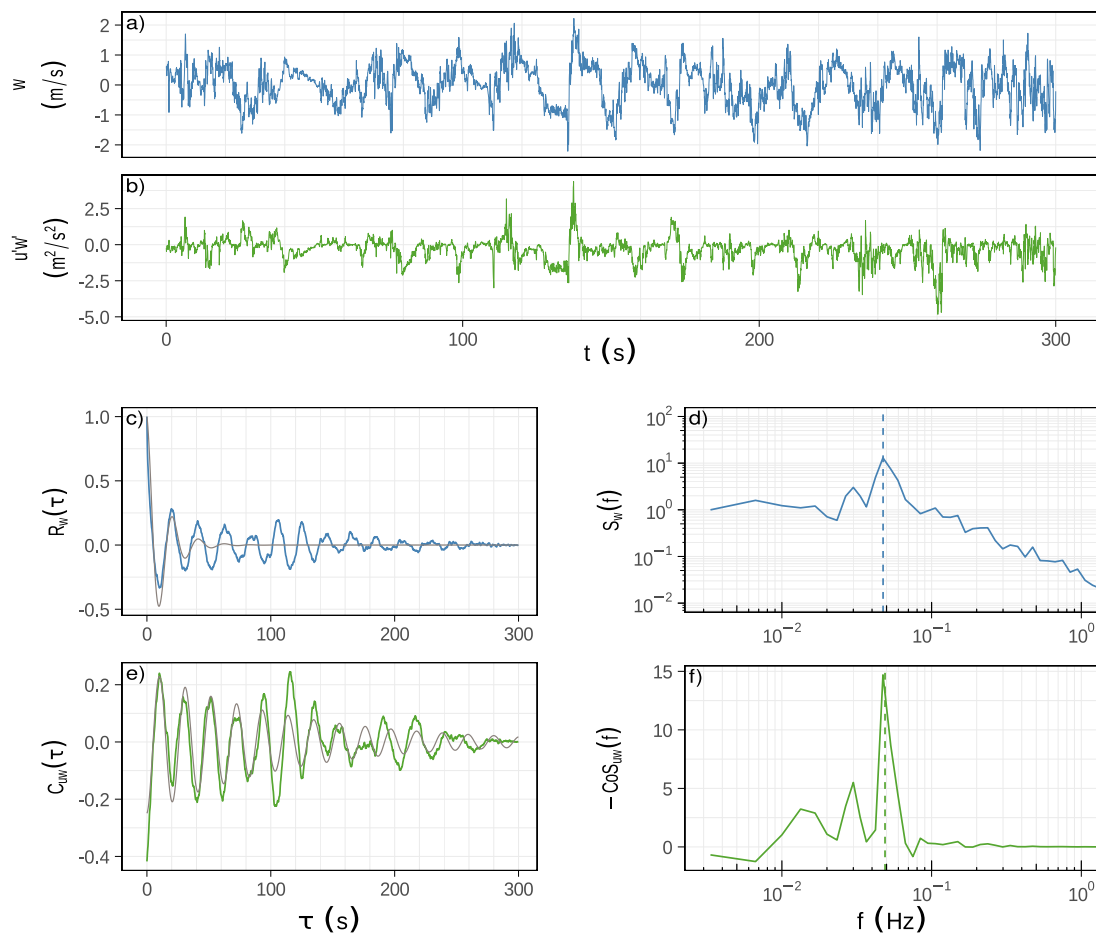
Fig. 2. Five minute time series (07:50–07:55, 31st August 2008) of w (a) and $u'w'$ (b) measured at 33 m in neutral conditions. Experimental autocorrelation function (c: blue line) and cross-correlation function (e: green) together with their fits represented by Eqs. (1) and (2), respectively (thick grey lines). Experimental w-spectrum (d) and $u'w'$ co-spectrum (f) corresponding to the time series shown in panels (a) and (b). The vertical dashed lines refer to the frequency f_{peak} detected by Eq. (5).
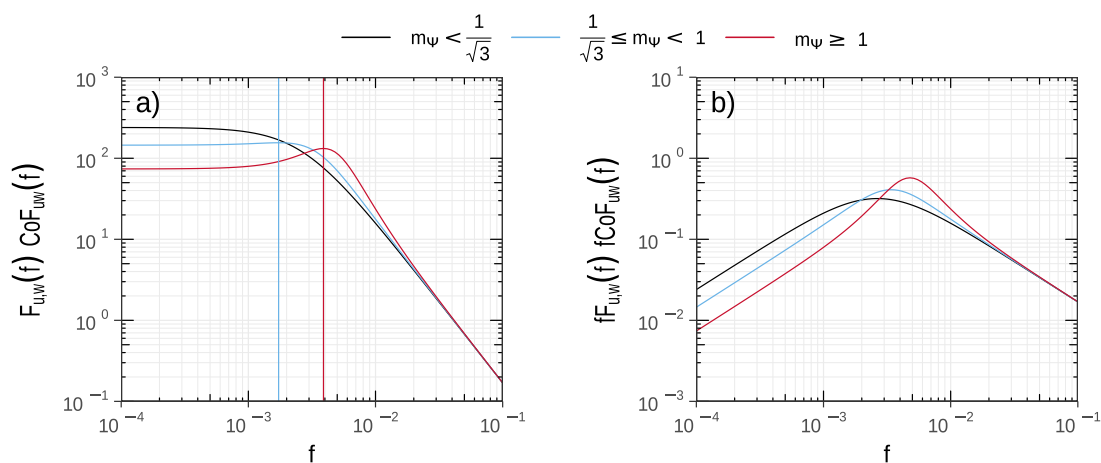

Fig. 3. Log–log representation of the (a) unweighted and (b) frequency-weighted spectra and cospectra (Eqs. (3) and (4)) for $p_\psi = \frac{1}{60}\,\mathrm{s}^{-1}$ and $m_\psi = 0, \frac{1.4}{\sqrt{3}}, 1.5$ (black, blue and red lines, respectively). The vertical lines identify f_{peak} (Eq. (5)).

step the anemometric data were rotated into the streamwise system and the mean vertical wind component was removed (double rotation, McMillen, 1988).

The identification of atmospheric stability classes was performed on the basis of the behaviour of the main turbulent statistics close to the top of the forest (Dupont and Patton, 2012b; Cava et al., 2022). For this classification, the turbulent variables were evaluated choosing

two average time scales: 1 h for $z/L < 0$ and 5-min for $z/L > 0$. This criterium allows the capture of the actual turbulent contribution to micrometeorological statistics and to filter out the spurious contribution due to submeso activity in stable conditions (Vickers and Mahrt, 2006). Fig. 4 shows the kinematic heat flux ($\overline{w'T'}$), the kinematic momentum flux ($\overline{u'w'}$), the normalized vertical velocity standard deviation (σ_w/U_h) and the mean wind speed (U_h) as a function of the stability
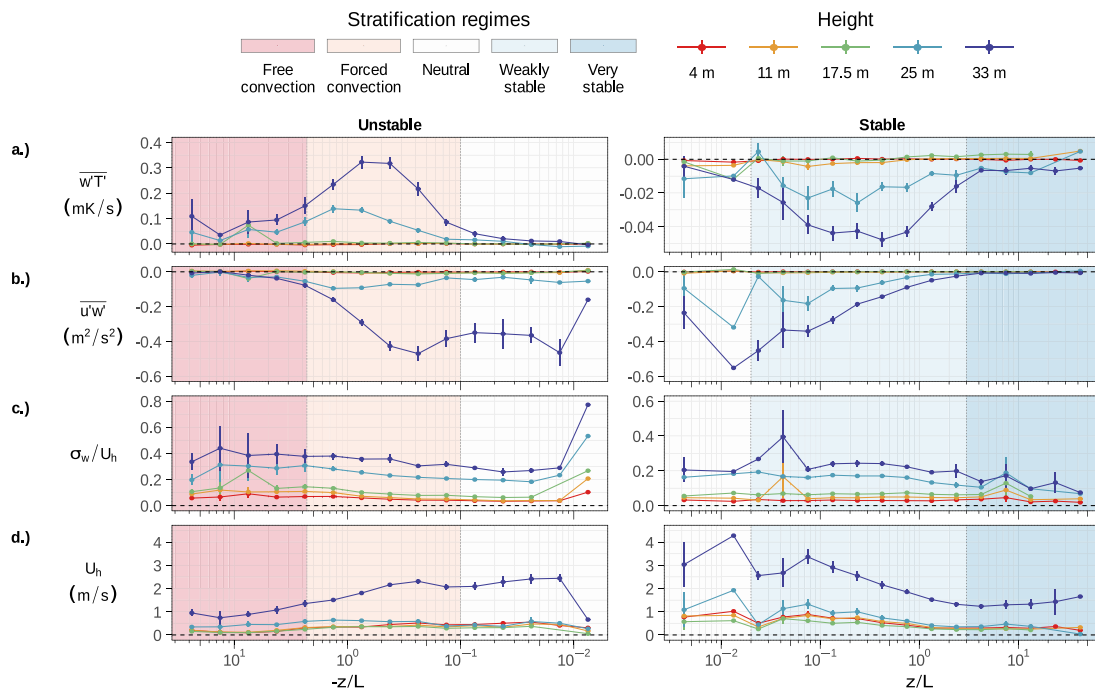
Fig. 4. Average values of the turbulent heat flux (a), momentum flux (b), normalized vertical velocity standard deviation (c) and wind velocity (d) computed at the different measurement levels as a function of the stability parameter z/L measured at $z = 33$ m. The vertical dotted lines and the shaded areas with different colours mark the stability regimes: free convection, forced convection, neutral (in the unstable and stable sides), weakly stable and very stable conditions. The vertical bars refer to the standard error of the mean.

parameter (z/L) measured at the highest level (close to the canopy top), where $z = 33$ m, $L = -(u_*^3 \overline{T})/(kg\overline{w'T'})$ is the Obukhov length, u_* is the friction velocity, k is the von Karman constant and g is the gravitational acceleration. Both L and u_* should refer to the canopy top and are, therefore, computed at the highest level (33 m). Hence, five stability regimes were identified, two unstable (free convection and forced convection), neutral (in unstable and stable sides), and two stable (weakly stable and very stable). Free convection regime ($z/L < -5$) is characterized by significant heat flux and vertical energy (σ_w/U_h), but very small momentum flux and weak wind speed ($U_h < 1.5$ ms^{-1}). Forced convection ($-5 \leq z/L < -0.1$) is characterized by the largest values of energy and turbulent heat and momentum fluxes and larger wind velocity ($U_h < 2.5$ ms^{-1}). In neutral regime ($-0.1 \leq z/L < 0.02$) wind intensity, vertical energy and momentum flux remain quite intense, while the heat flux collapses to zero and begins to grow again (in absolute value) in weakly stable conditions ($0.02 \leq z/L < 3$) characterized by large magnitudes of turbulent energy and fluxes and quite intense wind speed close the canopy top ($2 < U_h < 4$ ms^{-1}). In the very stable class, ($z/L \geq 3$) wind speed becomes weak and turbulent fluxes appear strongly reduced because inhibited by the negative buoyancy. Notably, forced convection and weakly stable regimes are the most frequent conditions during daytime and nighttime, respectively (not shown).

4.1. Methodology assessment

The correlation function methodology, proposed in Section 3, was applied to the experimental time series in order to investigate and compare the impact of coherent dynamics on the w spectrum and on the uw cospectrum shapes in the identified stability regimes. In this step of the analysis 5 min subsets were used for all stability classes with the aim of identifying oscillations with temporal scales compatible with mixing-layer CS. The procedure was largely tested by Mortarini et al. (2022) above an Amazon forest, and guarantees to filter our large-scale structures that could mask the CS dynamics. The w autocorrelation function and the uw cross correlation function were fitted using Eqs. (1)

and (2), respectively. Then the temporal scales of the CS (detected for $m_\Psi > \frac{1}{\sqrt{3}}$) were estimated using Eq. (5).

Fig. 5 shows the density histograms and the corresponding interpolated pdfs for T_{peak} of w spectra and uw cospectra, respectively, computed at the three highest measurement levels (17.5, 25, 33 m) in the five stability regimes. Table 1 shows the density peak values of $T_{\text{peak}_{w,uw}}$ for the same heights and stability conditions represented in Fig. 5. Notably, the T_{peak} pdfs display well defined maxima confined on temporal scales smaller than 100 s and very similar shapes along the different levels in forced convection, neutral and weakly stable stratifications. In these stability regimes both timescales increase inside the canopy, highlighting the effect of the crown area on the CS. Over the Amazon, Mortarini et al. (2022) found larger values of T_{peak_w}, this is expected for the larger height of the tropical forest. T_{peak_w} is related to the CS length-scale which in turn depends on the canopy depth. In free convection and very stable regimes the pfds have broader and less defined peaks because of the possible influence of larger scale motions. This is more evident in the T_{peak} pdf of uw because the momentum behaviour is influenced by the longitudinal velocity (u), which is more affected than the vertical velocity component (w) by large-scale motions (Mortarini et al., 2022). In all stability regimes at each height $T_{\text{peak}_{uw}}$ is considerably larger than T_{peak_w}, reflecting the influence of the horizontal velocity field on the momentum transport. The vertical evolution of spectral and cospectral energy showed in Cava et al. (2022) suggests that the fat tails in Fig. 5 may be due to the influence of inactive turbulence or of small convective plumes originating within the canopy in unstable conditions as well as to the interference of CS with horizontal submeso structures in very stable conditions. Hence, T_{peak_w} values far from the distribution peaks do not clearly represent CS. In the following of the analysis, $T_{\text{peak}_w} = 100$ s at 33 m will be used as a threshold value: subsets whose T_{peak_w} values exceed 100 s at 33 m and the respective subsets at lower levels will be disregarded. In forced convection and very stable stratification 100 s might be a strong constraint and it is worth of future investigations.

The value of the m parameter, representing the ratio between the time scale of fine-scale turbulence and the time scale of periodic
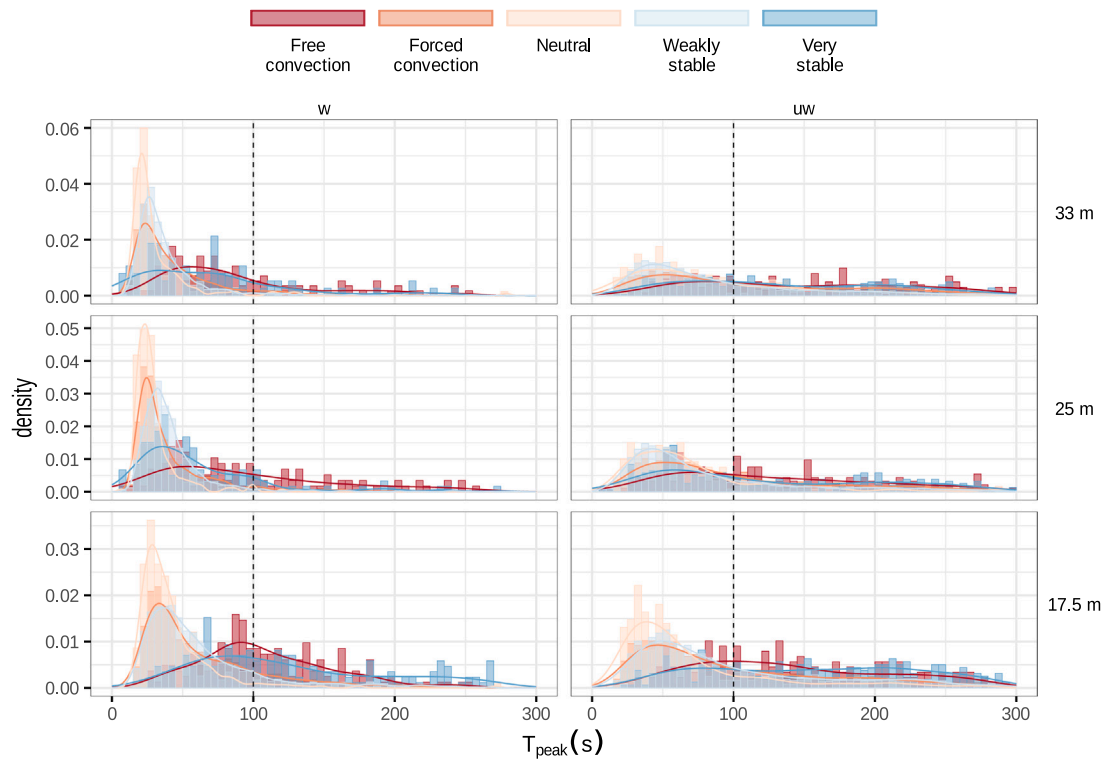
Fig. 5. T_{peak} density histograms and corresponding interpolated pdfs for w and uw (first and second column, respectively) at different measurement levels. The vertical dashed line refers to the 100 s threshold. Colours refer to the five stability regimes.

Table 1
Density peak values of $T_{peak_{w,uw}}$ evaluated according to Eq. (5) in the five stability regimes at 33, 25 and 17.5 m.

T_{peak} (s)	Free convection		Forced convection		Neutral		Weakly stable		Very stable	
	w	uw	w	uw	w	uw	w	uw	w	uw
33 m	56	83	24	55	21	47	26	46	34	80
25 m	54	74	24	51	23	48	33	42	36	64
17.5 m	90	102	37	49	28	40	37	49	83	200

oscillations (Mortarini et al., 2016, 2022), was used to discriminate between data subsets where coherent structures were absent (m_w = NA, i.e. Not Available) and data subsets in which the flow was characterized by them ($m_w > 1$). Spectra relative to the two end members exhibit a different behaviour mainly in the region of energy production (as shown in Fig. 6). In the first class (m_w = NA), both above and inside the crown, spectra exhibit the shape typical of fine-scale turbulence in the inertial sublayer in each stability regimes; i.e. a broad maximum at large-scale and a clear energy cascade in the inertial subrange ($\tilde{f}^{-5/3}$). On the other hand, in the second class ($m_w > 1$), spectra have a well defined and narrow peak at f_{peak_w} (identified using the autocorrelation method, Eq. (5)) and showing a $\tilde{f}^{-2}$ decay typical of oscillating functions in the proximity of the peak region (see Fig. 3). This indicates that the energy production is mainly concentrated at the scale of the CS detected with Eq. (1); at smaller scales the energy drops following the K41 (Kolmogorov, 1941) power law ($\tilde{f}^{-5/3}$). The spectral behaviour appears similar in the different stability conditions and at the different levels except at $z = 17.5$ m, where a faster energy cascade ($\tilde{f}^{-2}$) is observed for $1 < \tilde{f} < 0.1$, suggestive of a dominance of coherent vortexes and a short-circuiting of energy produced by the interaction of coherent structures with the crown elements (Cava and Katul, 2008). Notably, the unconditioned average spectra (black lines in Fig. 6) show the influence of both flow structures detected by the correlation method able to discriminate between them.

The mean average uw cospectra (Fig. 7) show the same differences observed in the spectra at the production scales between the two classes of motions, but they appear noisier in particular at $z = 17.5$ m, where the momentum flux is largely absorbed by the forest crown (see Fig. 4). In the inertial subrange all the cospectra collapses and decay following the $-7/3$ power law. The unconditioned averaged cospectra (black lines) show the peak related to CS at almost all heights and stability conditions except in free convection and very stable at $z = 33$ m. This confirms the influence of coherent vortices on the momentum flux. However, as noticed discussing Fig. 5, the cospectral maxima in Fig. 7 might be influenced by horizontal structures (both coherent vortices or large-scale fluctuations) and not only by vertical coherent motions.

4.2. Turbulent vertical profiles

The application of the correlation methodology for the CS detection allows the investigation of the influence of different scales of motions on flow characteristics above and inside the forest. The detection of CS was performed using w autocorrelation. Vertical velocity auto-correlation functions were chosen, since they only take into account vertical coherent vortices, while the timescales identified by the uw cross-correlation function are influenced by horizontal structures and, in non-neutral conditions, by larger convective or submeso scales. As stated in the methodology assessment (4.1), the classification of turbulent structures corresponds to the two-end members shown in the w spectra (see Fig. 6): Coherent structures ($m_w > 1$) refer to 5 min time series with periodic behaviour and $T_{peak_w} < 100$ s, while
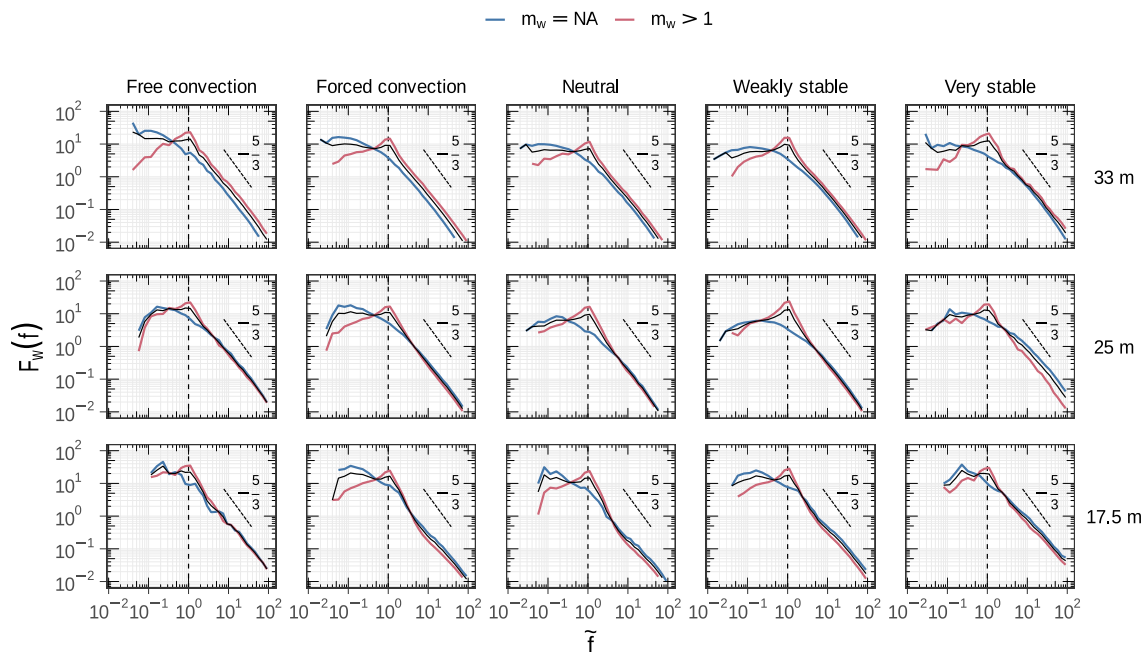
Fig. 6. Mean normalized w spectra, $F_w(f)$, as a function of the normalized frequency, $\tilde{f}$, for the two end members of the m_w classification: no fit (m_w = NA) or fine-scale turbulence (blue lines and $\tilde{f} = f \frac{z}{\bar{u}}$); and $m_w > 1$ and $T_{\text{peak}_w} < 100$ s or CS (red lines and $\tilde{f} = f \, T_{\text{peak}_w}$). Black lines refer to the unconditioned average spectra (mean of blue and red lines). The columns refer to different stability regimes, while the rows refer to different measurement levels.

Fig. 7. Mean normalized uw cospectra, $CoF_{uw}(f)$, as a function of the normalized frequency, $\tilde{f}$, for the two end members of the m_{uw} classifications: no fit (m_{uw} = NA) or fine-scale turbulence (blue lines $\tilde{f} = f \frac{z}{\bar{u}}$); and $m_{uw} > 1$ and $T_{\text{peak}_{uw}} < 100$ s or CS (red lines and $\tilde{f} = f \, T_{\text{peak}_{uw}}$). Black lines refer to the unconditioned average spectra (mean of blue and red lines). The columns refer to different stability regimes, while the rows refer to different measurement levels.
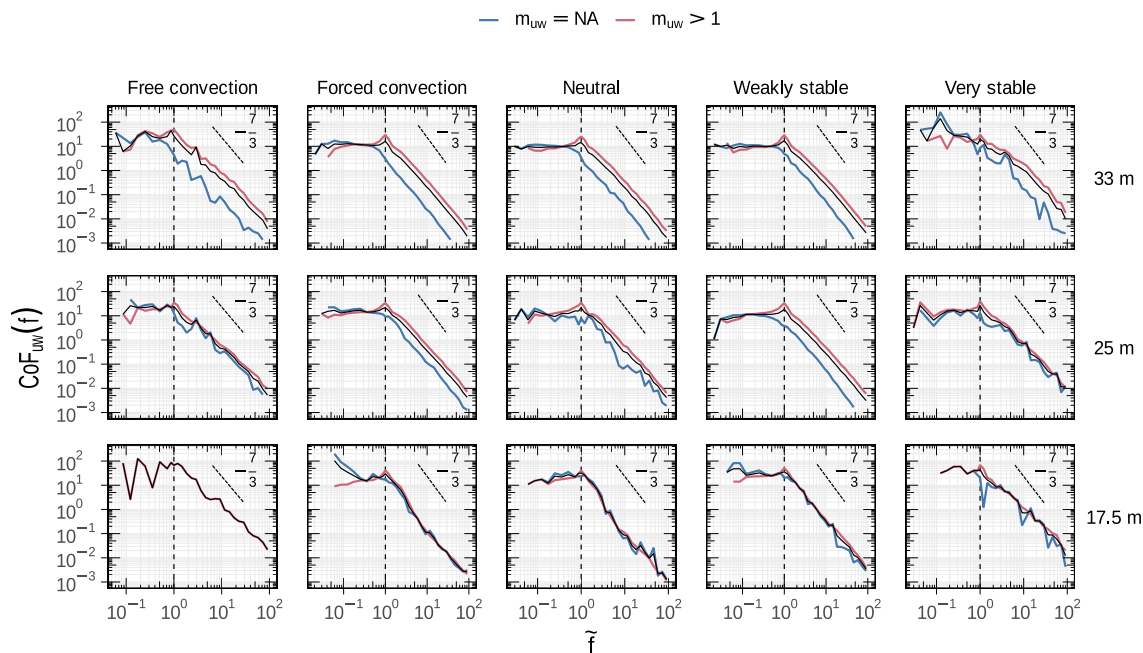
fine-scale turbulence (m_w = NA) refers to 5 min time series that do not exhibit periodic behaviour and consequently no fit was found. Those turbulent structures were selected on the basis of the results of autocorrelation methodology applied at the highest level (33 m) in order to use a coherent subset of data throughout the different levels. This criterion allows to study the propagation inside the forest of the structures detected at the canopy top.

Figs. 8 and 9 show the vertical profiles of the most typical canopy turbulent statistics for the different stability classes (shown in the multiple rows). In each panel the effect of distinct flow structures is shown: the contribution of CS (red lines), of fine-scale turbulence (blue lines) and the unconditioned averages (black lines) obtained using a temporal average of 1 h for free and forced convection and 5 min for neutral and stable regimes. In particular, the comparison in unstable conditions of the unconditioned averages with those conditioned by the two end-members (periodic structures and fine-scale turbulence) allows to distinguish the effect of CS and from that of larger scales (such as thermal structures) which cannot be resolved using the short time window used for computing the 'conditioned' statistics.
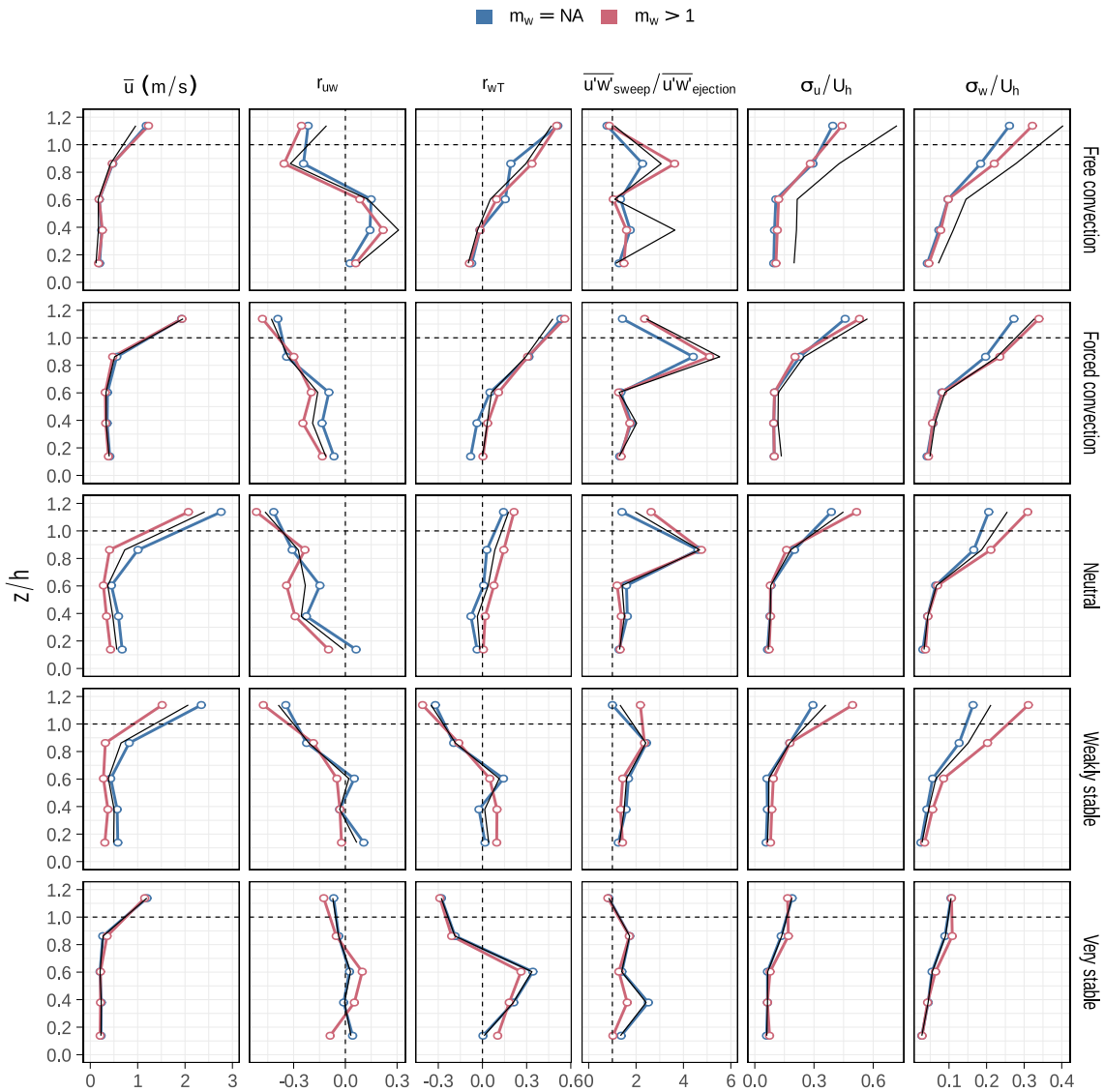
Fig. 8. Turbulence family portrait showing profiles with normalized height z/h at each stability class: $\bar{u}$, r_{uw}, r_{wT}, $\overline{u'w'}_{sweep}/\overline{u'w'}_{ejection}$, σ_u/U_h σ_w/U_h where $U_h = \bar{u}(h)$ and $h = 28$ m is the height of the canopy. Red lines refer to $m_w > 1$ and $T_{peak_w} < 100$ s, while blue lines refer to available no fit (m = NA). Black lines refer to the unconditioned averages with a temporal average of 1 h for free and forced convection and 5 min for neutral and stable regimes.

The wind speed (shown in the first column of Fig. 8) exhibits a rapid decay in respect to the value observed close to the canopy top. The strong shear just above and in the upper part of the forest results in an inflection point at the forest–atmosphere interface (Raupach et al., 1996). In free convection and very stable stratification, the wind speed assumes its smallest value at the canopy top (≈ 1.5 ms^{-1}), presenting almost no difference for the two constraining cases. This underlines the almost negligible role of wind shear in both free convection and very stable cases. Confirming the results of Dias-Júnior et al. (2013) and Thomas et al. (2006), the small vertical velocity gradient at the canopy top results in a less evident inflection point and is associated to the attenuation of coherent vortices in the RSL. On the contrary, in all the other stability conditions (in particular in neutrality and weakly stable stratifications) the profiles associated with the presence of CS present slightly weaker winds and stronger shear at the canopy top.

The correlation coefficients measure the turbulence ability in transferring momentum flux ($r_{uw} = \overline{u'w'}/(\sigma_u\sigma_w)$, second column in Fig. 8) or heat flux ($r_{wT} = \overline{w'T'}/(\sigma_w\sigma_T)$, third column in Fig. 8) inside the vegetation. As observed in the typical RSL profiles found in literature (see Brunet, 2020, for a review), the largest values of correlations are observed in the highest part of the forest, then they decrease and display

differences related to the stability conditions and to the kind of flow structures responsible for the transport. The comparison of the profiles of the two end-members highlights the highest efficiency of CS (red lines) in transferring momentum and heat. Moreover, in all stability conditions the CS appear more energetic than fine-scale turbulence (blue lines), as shown in the vertical profiles of the normalized wind standard deviations (fifth and sixth columns in Fig. 8). As already observed elsewhere (Cava et al., 2022), the flow inside the canopy appears mainly modulated by sweeps ($Sk_u > 0$ and $Sk_w < 0$, first and second rows of Fig. 9) that dominate the transport ($\overline{u'w'}_{sweep}/\overline{u'w'}_{ejection} > 1$, fourth column in Fig. 8), characterized by a high intermittency as indicated by the values of kurtosis larger than the typical Gaussian value ($K = 3$) (third and fourth rows of Fig. 9). In the crown region, the sweep contribution to momentum transport appears largest in unstable and neutral conditions ($\overline{u'w'}_{sweep}/\overline{u'w'}_{ejection} > 4$), whereas is halved in stable regimes. More, the sweeps appear more intense ($Sk_u \approx 0.8$ and $Sk_w \approx -1$) and intermittent (K_u and $K_w \approx 5$) in forced convection and neutral regimes. In the trunk space the role of ejections and sweeps tends to balance $\overline{u'w'}_{sweep}/\overline{u'w'}_{ejection} \approx 1$ and the degree of the structure intermittency decreases.
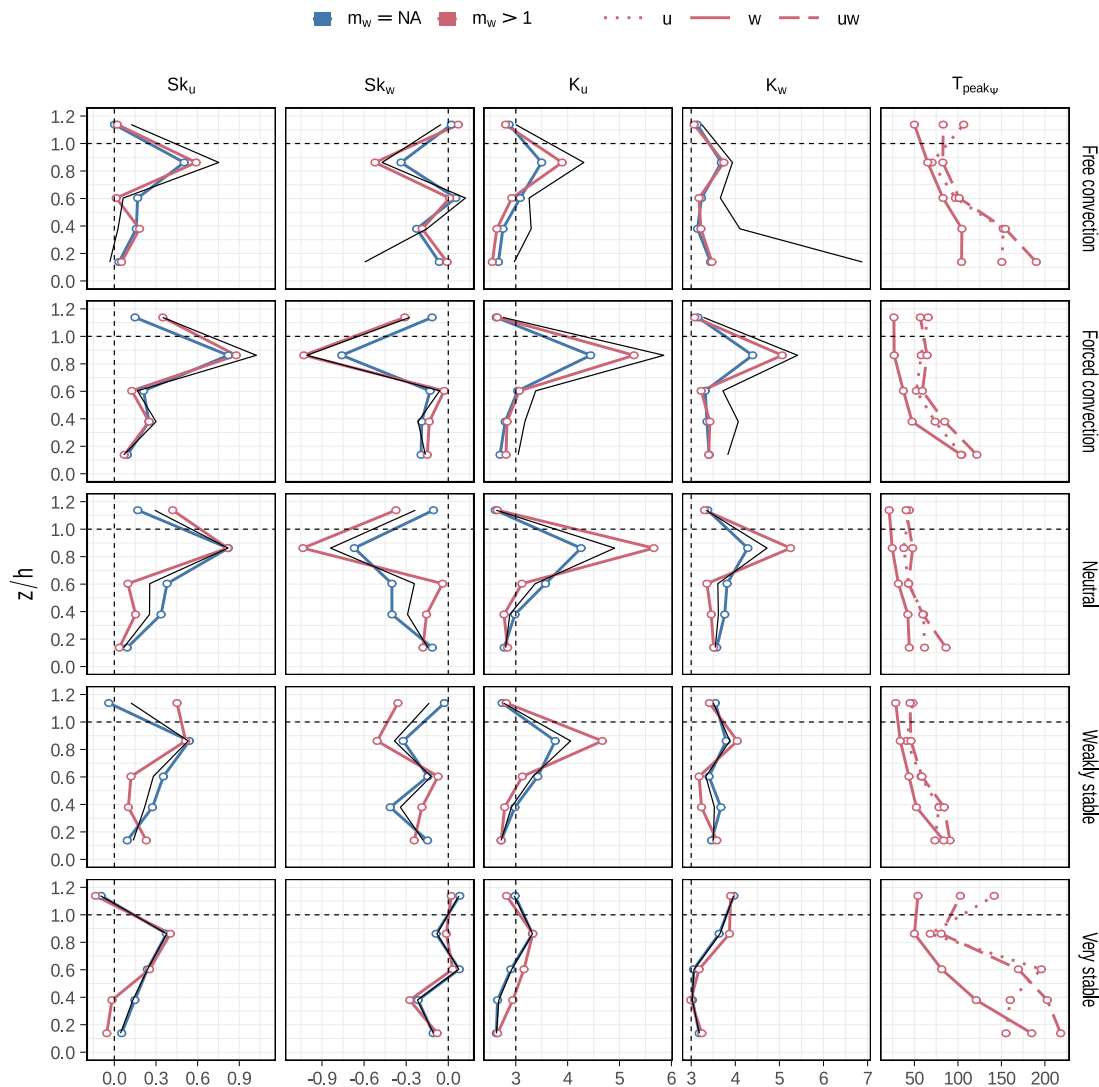
Fig. 9. Same as Fig. 8 for Sk_u, Sk_w, K_u, K_w, and the median of the temporal scales T_{peak} (Eq. (5)) for u (dotted line), w (continuous line) and uw (dashed line).

The characteristics of turbulent profiles in very stable stratification are similar to those observed in other regimes, but CS appear less energetic and less intermittent. Notably, the momentum and heat fluxes reverse their signs in the trunk space indicating that the weak CS generated at the canopy top are unable to penetrate in the deepest layers of the forest with a consequent decoupling of the flow in very stable conditions (see also Dupont and Patton, 2012b; Cava et al., 2022). In this regime the unconditioned profiles of normalized standard deviations (fifth and sixth columns in Fig. 8) and of higher moments (skewnesses and kurtoses, shown in Fig. 9) display the highly intermittent intrusions of large-scale and energetic sweeps inside the forest. Even if weaker, this effect can also be observed in forced convection regime.

The last column of Fig. 9 shows the median vertical profiles of the spectral (T_{peak_u}, T_{peak_w}) and cospectral ($T_{peak_{uw}}$) peak values (Eq. (5)), only cases with $m_w > 1$ are considered. As depicted in Fig. 5, both time scale distributions have a positive skewness (more evident for forced, neutral and weakly conditions), i.e. extreme values of T_{peak} affect the mean more than the median. Since our interest is centred on the characteristic time scales of CS, the median was chosen as the best descriptor of central tendency in these asymmetric distributions. It is very interesting how in neutral, weakly stable and forced convection stratification the most energetic timescale for the momentum flux is associated to the longitudinal scale of the CS and not to their vertical at

all measurements heights but 4 m. Close to the ground the momentum flux exceeds both the horizontal and the vertical time scales. On the other hand, just outside the canopy the time scale of the momentum flux in both free convection and very stable conditions is larger than T_{peak_w} and smaller of T_{peak_u}. This may explain the poor performance of Eq. (4) (see also Fig. 7) in these conditions. During free convection and very stable regimes, the momentum transport is mainly influenced by convective and submeso structures, respectively. Hence, CS are more rare and intermittent, while the cross-correlation function does not identify a clear peak (Fig. 3, right panels). All the T_{peak} values become larger while propagating downward inside the canopy. Coherent vortices produced at the canopy top have dimensions comparable to the canopy height. Thus, if we assume that their length-scale can be evaluated from the Taylor hypothesis as $\bar{u}\, T_{peak}$, as $\bar{u}$ rapidly reduces with height inside the canopy T_{peak} needs to grow to preserve the coherent structures spatial length-scale.

4.3. Coherent structures contribution to turbulent exchange

The estimate of CS contribution to the turbulent transport is one of the main goals in the RSL research, in particular above forested sites (Gao et al., 1989; Collineau and Brunet, 1993b; Lu and Fitzjarrald, 1994; Thomas and Foken, 2005, 2007; Barthlott et al., 2007; Serafimovich et al., 2011). Differences in the definition of flux contribution
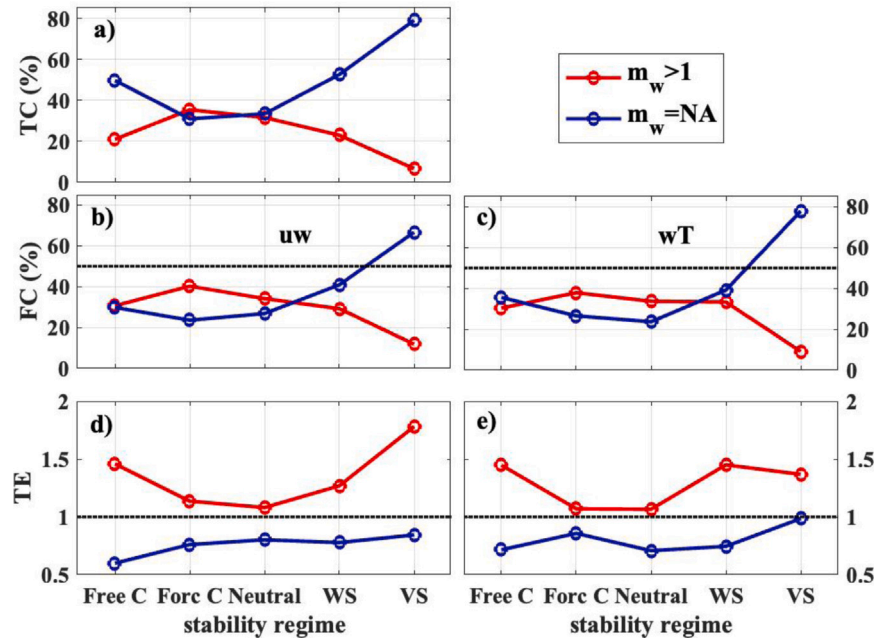
Fig. 10. Average values in different stability regimes of time cover (a, Eq. (6)), coherent structures contribution to the transport (Eq. (7)) and transport efficiency (Eq. (8)) for momentum flux (b, d) and for heat flux (c, e), respectively. Red lines refer to coherent structures ($m_w > 1$ and $T_{\text{peak}_w} < 100$ s) while blue lines refer to fine-scale turbulence (no fit, $m_w = $ NA) detected at 33 m.

depend on the methodology used to detect the CS (Barthlott et al., 2007). In this work flux contribution was estimated adapting (Lu and Fitzjarrald, 1994) definitions to the autocorrelation methodology.

The net time cover (TC) of detected structures represents the percentage of 5 min subsets with active coherent structures in the overall data set:

$$TC = \frac{N_{\text{CS}}}{N_{\text{tot}}}(\%) \tag{6}$$

where N_{CS} is the number of 5 min time series where the coherent structures were active ($m_w > 1$ and $T_{\text{peak}_w} < 100$ s) and N_{tot} is the total number of 5 min subsets in the data set. The contribution of coherent structures to the turbulent flux (FC) and their transport efficiency (TE) are, respectively, defined as:

$$FC = \left(\frac{1}{N_{\text{CS}}}\sum_{k=1}^{N_{\text{CS}}} F_k\right)\bigg/\left(\frac{1}{N}\sum_{i=1}^{N} F_i\right)(\%) \tag{7}$$

$$TE = \frac{FC}{TC} \tag{8}$$

where F_i is the mean turbulent flux in the ith 5 min time series and F_k is the mean turbulent flux in the ith 5 min time series with active CS. TE values greater (lower) than 1 indicate efficiency (inefficiency) of CS in the turbulent transport. The same parameters can be defined for fine-scale turbulence subsets ($m = $ NA).

In Fig. 10 the average values of time cover, contribution to momentum and heat turbulent fluxes and correspondent transport efficiencies relative to both CS and fine-scale turbulence are shown in the different stability regimes. The proposed detection methodology revealed an average time occurrence of CS that not exceeded 40% in all stability regimes. The lowest values are attained in free convection and stable regimes. In very stable conditions the CS remain active only 10% of the total time, confirming their weak contribution to the momentum transport (Figs. 8 and 9 and relative discussion). The time cover of fine-scale turbulence exhibits a specular trend with the maximum value in very stable atmospheric stratification ($\approx 80\%$). It is important to clarify that the percentages do not sum to 100% since uncertain cases ($m < 1$) are not plotted, in order to have a clear comparison between the role of coherent and incoherent structures in the turbulent transport.

In agreement with (Barthlott et al., 2007) who observed an increasing flux contribution with increasing time cover, the contribution to the momentum and heat fluxes by different structures follows the same behaviour of TC. The CS contributions for momentum flux lie between 30%–40%, dropping to 7% in very stable case, where CS remain active for only 10% of the total time. A similar trend is observed for heat flux. These values are in agreement with other results found in literature (Collineau and Brunet, 1993b; Lu and Fitzjarrald, 1994; Barthlott et al., 2007). Fig. 10d display a large transport efficiency of CS ($TE > 1$) for all stability regimes. On the other hand, TE for fine-scale turbulence attains low values ($TE < 1$) remarking the relatively poor efficiency of incoherent eddies in turbulent transport although their comparable or higher values of time cover. This result confirms the importance of CS in the transport processes above vegetated canopy.

5. Conclusions

The aim of this work was to investigate the impact of coherent structures on the RSL flow dynamics, and on the exchange processes at the canopy–atmosphere interface in different atmospheric stratification conditions. A dataset collected within an uneven-aged mixed coniferous forest on an Alpine Plateau (Lavarone, Italy), during a summertime intensive measurement campaign, was used for the analysis. Five different stability regimes, from free convection to very stable stratification, were defined. The detection of CS and their characteristic timescales were accomplished by fitting the vertical velocity auto-correlation function with an oscillating decaying function. The auto-correlation function methodology was extended to cross-correlation functions, proposing an original theoretical form for the cross-correlation function of turbulent fluxes in that atmospheric flow presents a periodic behaviour. The proposed methodology represents a new and alternative pathway for assessing the presence and the influence of CS in the atmospheric flow at the canopy–forest interface. The value of the m parameter, (that represents the ratio between the time scale of fine-scale turbulence and the time scale of periodic oscillations), was used to discriminate between data subsets where coherent structures were absent ($m_w = $ NA, i.e. Not Available) from data subsets in which the flow was characterized by them ($m_w > 1$).

Average spectra and cospectra of the two *m*-classes presented different behaviours in the energy production region. For fine-scale turbulence, they exhibited a broad maximum, while for CS, a well defined and narrow peak was evident at a frequency correspondent to the temporal scale identified by the correlation methodology. On the other hand, close to the spectral peak a -2 slope in the energy cascade evidences the dominance of CS on the flow dynamics, at smaller scales both flow structures exhibit the inertial range power law ($\tilde{f}^{-5/3}$, Kolmogorov, 1941). The presence of CS is associated with larger vertical velocity gradients and slightly weaker winds, resulting in smaller shear length scales at the canopy top.

In neutral, weakly stable and forced convection regimes, CS manifested themselves inside the forest as energetic and intermittent sweeps very efficient in the transport of momentum and heat. Farther from neutrality, their influence on the atmospheric flow was reduced and less evident. As a matter of fact, in free convection and very stable regimes, CS appear less energetic and less efficient in the transport inside the forest. The sign reversal of the momentum fluxes disclosed the inability of such structures to reach the deepest layers of the canopy and the decoupling of the flow between the upper and lower levels. The vertical time scale of coherent vortices is lower than their longitudinal timescale at all heights in all stability regimes. While the coherent vortices propagated downward, both the w and u timescales increased, probably trying to preserve the CS length scale as wind speed decayed inside the canopy. Close to neutrality (neutral, weakly stable and forced convection regimes), rather than the vertical component, is the longitudinal velocity that appears to modulate the momentum flux timescale. Since free convection and very stable regimes showed to be less apt to the development of coherent structures, the momentum transport was modulated by larger scales such as thermal structures and submeso motions.

The contribution to momentum and heat fluxes of both CS and fine-scale turbulence increases with increasing time cover. The maximum flux contributions are attained in neutral conditions or in moderately stable and unstable regimes and do not exceed 40%. In free convection and very stable stratifications, the contributions of turbulent fluxes drop, reaching their minimum value in very stable regimes ($< 10\%$). However, even in the two extreme stratification regimes transport efficiency associated to CS remains larger than 1. Fine-scale turbulence, in spite of similar or larger time cover, showed poor transport efficiency. Finally, the obtained results demonstrated the EAF methodology efficiency in a clear and fast detection of CS when compared to wavelet algorithms that are usually applied to window larger than 5 min and that may lead to erroneous results in presence of superimposition of flow motions characterized by different scales.

Declaration of competing interest

The authors declare that they have no known competing financial interests or personal relationships that could have appeared to influence the work reported in this paper.

Data availability

Data will be made available on request.

Acknowledgments

References

Allouche, M., Bou-Zeid, E., Ansorge, C., Katul, G.G., Chamecki, M., Acevedo, O., Thanekar, S., Fuentes, J.D., 2022. The detection, genesis, and modeling of turbulence intermittency in the stable atmospheric surface layer. J. Atmos. Sci. 79, 1171–1190.

Anfossi, D., Oettl, D., Degrazia, G., Goulart, A., 2005. An analysis of sonic anemometer observations in low wind speed conditions. Bound.-Layer Meteorol. 114, 179–203.

Ansorge, C., Mellado, J.P., 2014. Global intermittency and collapsing turbulence in the stratified planetary boundary layer. Bound.-Layer Meteorol. 153, 89–116.

Ansorge, C., Mellado, J.P., 2016. Analyses of external and global intermittency in the logarithmic layer of Ekman flow. J. Fluid Mech. 805, 611–635.

Antonia, R.A., 1981. Conditional sampling in turbulence measurement. Annu. Rev. Fluid Mech. 13, 131–156. http://dx.doi.org/10.1146/annurev.fl.13.010181.001023.

Barthlott, C., Drobinski, P., Fesquet, C., Dubos, T., Pietras, C., 2007. Long-term study of coherent structures in the atmospheric surface layer. Bound.-Lay. Meteorol. 125, 1–24. http://dx.doi.org/10.1007/s10546-007-9190-9.

Bergström, H., Högström, U., 1989. Turbulent exchange above a pine forest II. Organized structures. Bound.-Lay. Meteorol. 49, 231–263. http://dx.doi.org/10.1007/BF00120972.

Brunet, Y., 2020. Turbulent flow in plant canopies: Historical perspective and overview. Bound.-Lay. Meteorol. 177, 315–364. http://dx.doi.org/10.1007/s10546-020-00560-7.

Brunet, Y., Irvine, M.R., 2000. The control of coherent eddies in vegetation canopies: Streamwise structure spacing, canopy shear scale and atmospheric stability. Bound.-Lay. Meteorol. 94, 139–163. http://dx.doi.org/10.1023/A:1002406616227.

Cava, D., Dias-Júnior, C.Q., Acevedo, O., Oliveira, P.E.S., Tsokankunku, A., Sörgel, M., Manzi, A.O., de Araújo, A.C., Brondani, D.V., Toro, I.M.C., Mortarini, L., 2022. Vertical propagation of submeso and coherent structure in a tall and dense Amazon forest in different stability conditions PART I: Flow structure within and above the roughness sublayer. Agricult. Forest Meteorol. 322, 108983. http://dx.doi.org/10.1016/j.agrformet.2022.108983.

Cava, D., Giostra, U., Siqueira, M., Katul, G., 2004. Organised motion and radiative perturbations in the nocturnal canopy sublayer above an even-aged pine forest. Bound.-Lay. Meteorol. 112, 129–157.

Cava, D., Katul, G.G., 2008. Spectral short-circuiting and wake production within the canopy trunk space of an alpine hardwood forest. Bound.-Lay. Meteorol. 126, 415–431. http://dx.doi.org/10.1007/s10546-007-9246-x.

Cava, D., Katul, G.G., Scrimieri, A., Poggi, D., Cescatti, A., Giostra, U., 2006. Buoyancy and the sensible heat flux budget within dense canopies. Bound.-Lay. Meteorol. 118, 217–240. http://dx.doi.org/10.1007/s10546-005-4736-1.

Chen, J.M., Black, T.A., 1992. Defining leaf area index for non-flat leaves. Plant Cell Environ. 15, 421–429. http://dx.doi.org/10.1111/j.1365-3040.1992.tb00992.x.

Chen, W., Novak, M.D., Black, T.A., Lee, X., 1997. Coherent eddies and temperature structure functions for three contrasting surfaces. Part I: Ramp model with finite microfront time. Bound.-Lay. Meteorol. 84, 99–124. http://dx.doi.org/10.1023/A:1000338817250.

Chor, T.L., Dias, N.L., Araújo, A., Wolff, S., Zahn, E., Manzi, A., Trebs, I., Sá, M.O., Teixeira, P.R., Sörgel, M., 2017. Flux-variance and flux-gradient relationships in the roughness sublayer over the Amazon forest. Agricult. Forest Meteorol. 239, 213–222.

Collineau, S., Brunet, Y., 1993a. Detection of turbulent coherent motions in a forest canopy part I: Wavelet analysis. Bound.-Lay. Meteorol. 65, 357–379. http://dx.doi.org/10.1007/BF00707033.

Collineau, S., Brunet, Y., 1993b. Detection of turbulent coherent motions in a forest canopy part II: Time-scales and conditional averages. Bound.-Lay. Meteorol. 66, 49–73. http://dx.doi.org/10.1007/BF00705459.

Daubechies, I., 1992. Ten Lectures on Wavelets. In: CBMS-NSF Regional Conference Series in Applied Mathematics, vol. 61, Society for Industrial and Applied Mathematics, Philadelphia, PA.

Dias-Júnior, C.Q., Marques Filho, E.P., Sá, L.D.A., 2015. A large eddy simulation model applied to analyze the turbulent flow above Amazon forest. J. Wind Eng. Ind. Aerodyn. 147, 143–153. http://dx.doi.org/10.1016/j.jweia.2015.10.003.

Dias-Júnior, C.Q., Sá, L.D.A., Marques Filho, E.P., Santana, R.A., Mauder, M., Manzi, A.O., 2017. Turbulence regimes in the stable boundary layer above and within the Amazon forest. Agricult. Forest Meteorol. 233, 122–132.

Dias-Júnior, C.Q., Sá, L.D.A., Pachêco, V., de Souza, C., 2013. Coherent structures detected in the unstable atmospheric surface layer above the Amazon forest. J. Wind Eng. Ind. Aerodyn. 115, 1–8.

Drobinski, P., Carlotti, P., Redelsperger, J.-L., Bantad, R., Masson, V., Newsom, R., 2007. Numerical and experimental investigation of the neutral atmospheric surface layer. J. Atmos. Sci. 64, 137–156. http://dx.doi.org/10.1175/JAS3831.1.

Dunyak, J., Gilliam, X., Peterson, R., Smith, D., 1998. Coherent gust detection by wavelet transform. J. Wind Eng. Ind. Aerodyn. 77, 467–478.

Dupont, S., Patton, E.G., 2012a. Influence of stability and seasonal canopy changes on micrometeorology within and above an orchard canopy: The CHATS experiment. Agricult. Forest Meteorol. 157, 11–29. http://dx.doi.org/10.1016/j.agrformet.2012.01.011.

Dupont, S., Patton, E.G., 2012b. Momentum and scalar transport within a vegetation canopy following atmospheric stability and seasonal canopy changes: The CHATS experiment. Atmos. Chem. Phys. 12, 5913–5935.

Dwyer, M.J., Patton, E.G., Shaw, R.H., 1997. Turbulent kinetic energy budgets from a large-eddy simulation of airflow above and within a forest canopy. Bound.-Lay. Meteorol. 84, 23–43. http://dx.doi.org/10.1023/A:1000301303543.

Farge, M., 1992. Wavelet transforms and their applications to turbulence. Annu. Rev. Fluid Mech. 24, 395–458.

Feigenwinter, C., Vogt, R., 2005. Detection and analysis of coherent structures in urban turbulence. Theor. Appl. Climatol. 81, 219–230. http://dx.doi.org/10.1007/s00704-004-0111-2.

Finnigan, J., 2000. Turbulence in plant canopies. Annu. Rev. Fluid Mech. 32, 519–571. http://dx.doi.org/10.1146/annurev.fluid.32.1.519.

Finnigan, J.J., Shaw, R.H., Patton, E.G., 2009. Turbulence structure above a vegetation canopy. J. Fluid Mech. 637, 387–424. http://dx.doi.org/10.1017/S0022112009990589.

Foster, R.C., Vianey, F., Drobinski, P., Carlotti, P., 2006. Near-surface coherent structures and the vertical momentum flux in a large-eddy simulation of the neutrally-stratified boundary layer. Bound.-Lay. Meteorol. 120, 229–255. http://dx.doi.org/10.1007/s10546-006-9054-8.

Gao, W., Shaw, R.H., Paw U., K.T., 1989. Observation of organized structure in turbulent flow within and above a forest canopy. Bound.-Lay. Meteorol. 47, 349–377. http://dx.doi.org/10.1007/BF00122339.

Harman, I.N., Finnigan, J.J., 2007. A simple unified theory for flow in the canopy and roughness sublayer. Bound.-Lay. Meteorol. 123, 339–363. http://dx.doi.org/10.1007/s10546-006-9145-6.

Harman, I.N., Finnigan, J.J., 2008. Scalar concentration profiles in the canopy and roughness sublayer. Bound.-Lay. Meteorol. 129, 323–351. http://dx.doi.org/10.1007/s10546-008-9328-4.

Kaimal, J.C., Finnigan, J.J., 1994. Atmospheric Boundary Layer Flows: Their Structure and Measurement. Oxford University Press.

Katul, G.G., Cava, D., Siqueira, M., Poggi, D., 2013. Scalar turbulence within the canopy sublayer. In: Coherent Flow Structures at Earth's Surface. John Wiley & Sons, Ltd, pp. 73–95. http://dx.doi.org/10.1002/9781118527221.ch6.

Kolmogorov, A.N., 1941. Local structure of turbulence in incompressible viscous fluid for very large Reynolds number. Dokl. Akad. Nauk SSSR 30, 299–301.

Launiainen, S., Veasal, T., Mölder, M., Mammarella, I., Smolander, S., Rannik, Ü., Kolari, P., Hari, P., Lindroth, A., Katul, G.G., 2007. Vertical variability and effect of stability on turbulence characteristics down to the floor of a pine forest. Tellus B 59, 919–936. http://dx.doi.org/10.1111/j.1600-0889.2007.00313.x.

Lee, X., Baar, A.G., 1998. Climatology of gravity waves in a forest. Q. J. R. Meteorol. Soc. 124, 1403–1419. http://dx.doi.org/10.1002/qj.49712454904.

Lu, C.-H., Fitzjarrald, D.R., 1994. Seasonal and diurnal variations of coherent structures over a deciduous forest. Bound.-Lay. Meteorol. 69, 43–69.

Marcolla, B., Pitacco, A., Cescatti, A., 2003. Canopy architecture and turbulence structure in a coniferous forest. Bound.-Lay. Meteorol. 108, 39–59. http://dx.doi.org/10.1023/A:1023027709805.

McMillen, R.T., 1988. An eddy correlation technique with extended applicability to non-simple terrain. Bound.-Lay. Meteorol. 43, 231–245.

Mortarini, L., Cava, D., Giostra, U., Costa, F.D., Degrazia, G., Anfossi, D., Acevedo, O., 2019. Horizontal meandering as a distinctive feature of the stable boundary layer. J. Atmos. Sci. 76, 3029–3046. http://dx.doi.org/10.1175/JAS-D-18-0280.1.

Mortarini, L., Dias-Júnior, C.Q., Acevedo, O., Oliveira, P.E.S., Tsokankunku, A., Sörgel, M., Manzi, A.O., de Araújo, A.C., Brondani, D.V., Toro, I.M.C., Giostra, U., Cava, D., 2022. Vertical propagation of submeso and coherent structure in a tall and dense amazon forest in different stability conditions. PART II: Coherent structures analysis. Agricult. Forest Meteorol. 322, 108993. http://dx.doi.org/10.1016/j.agrformet.2022.108993.

Mortarini, L., Katul, G., Cava, D., Dias-Júnior, C.Q., Diaz, N., Chamecki, M., 2023. Adjustments to the law-of-the wall above an Amazon forest explained by a spectral link.

Mortarini, L., Maldaner, S., Moor, L.P., Stefanello, M.B., Acevedo, O., Degrazia, G., Anfossi, D., 2016. Temperature auto-correlation and spectra functions in low-wind meandering conditions. Q. J. R. Meteorol. Soc. 142, 1881–1889. http://dx.doi.org/10.1002/qj.2796, arXiv:https://rmets.onlinelibrary.wiley.com/doi/pdf/10.1002/qj.2796.

Oliveira, P.E.S., Acevedo, O.C., Sörgel, M., Tsokankunku, A., Wolff, S., Araújo, A.C., Souza, R.A.F., Sá, M.O., Manzi, A.O., Andreae, M.O., 2018. Nighttime wind and scalar variability within and above an amazonian canopy. Atmos. Chem. Phys. 18, 3083–3099. http://dx.doi.org/10.5194/acp-18-3083-2018.

Patton, E.G., P. P. Sullivan, R.H.S., Finnigan, J.J., Weil, J.C., 2016. Atmospheric stability influences on coupled boundary layer and canopy turbulence. J. Atmos. Sci. 73, 1621–1647. http://dx.doi.org/10.1175/JAS-D-15-0068.1.

Paw U, K.T., Brunet, Y., Collineau, S., Shaw, R.H., Maitani, T., Qiu, J., Hipps, L., 1992. On coherent structures in turbulence above and within agricultural plant canopies. Agricult. Forest Meteorol. 61, 55–68. http://dx.doi.org/10.1016/0168-1923(92)90025-Y.

Raupach, M.R., Finnigan, J.J., Brunet, Y., 1989. Coherent eddies in vegetation canopies. In: Proceedings of the Fourth Australian Conference on Heat and Mass Transfer, 9–12 May. Christchurch, New Zealand, 75–90 Christchurch, New Zealand, 75–90, pp. 75–90.

Raupach, M.R., Finnigan, J.J., Brunet, Y., 1996. Coherent eddies and turbulence in vegetation canopies; The mixing. Layer analogy. Bound.-Lay. Meteorol. 78, 351–382.

Raupach, M.R., Thom, A.S., 1981. Turbulence in and above plant canopies. Annu. Rev. Fluid Mech. 13, 97–129. http://dx.doi.org/10.1146/annurev.fl.13.010181.000525.

Robinson, S.K., 1991. Coherent motions in the turbulent boundary layer. Annu. Rev. Fluid Mech. 23, 601–639. http://dx.doi.org/10.1146/annurev.fl.23.010191.003125.

Santos, D.M., Acevedo, O.C., Chamecki, M., Fuentes, J., Gerken, T., Stoy, P.C., 2016. Temporal scales of the nocturnal flow within and above a forest canopy in amazonia. Bound.-Lay. Meteorol. 161, 73–98. http://dx.doi.org/10.1007/s10546-016-0158-5.

Serafimovich, A., Thomas, C., Foken, T., 2011. Vertical and horizontal transport of energy and matter by coherent motions in a tall spruce canopy. Bound.-Layer Meteorol. 140, 429.

Shaw, R.H., Brunet, Y., Finnigan, J.J., Raupach, M.R., 1995. A wind tunnel study of air flow in waving wheat: Two-point velocity statistics. Bound.-Lay. Meteorol. 76, 349–376. http://dx.doi.org/10.1007/BF00709238.

Su, H.-B., Shaw, R.H., Paw, K.T., Moeng, C.-H., Sullivan, P.P., 1998. Turbulent statistics of neutrally stratified flow within and above a sparse forest from large-eddy simulation and field observations. Bound.-Lay. Meteorol. 88, 363–397. http://dx.doi.org/10.1023/A:1001108411184.

Thomas, C., Foken, T., 2005. Detection of long-term coherent exchange over spruce forest using wavelet analysis. Theor. Appl. Climatol. 80, 91–104. http://dx.doi.org/10.1007/s00704-004-0093-0.

Thomas, C., Foken, T., 2007. Organised motion in a tall spruce canopy: Temporal scales, structure spacing and terrain effects. Bound.-Lay. Meteorol. 122, 123–147. http://dx.doi.org/10.1007/s10546-006-9087-z.

Thomas, C., Mayer, J.-C., Meixner, F.X., Foken, T., 2006. Analysis of low-frequency turbulence above tall vegetation using a Doppler sodar. Bound.-Lay. Meteorol. 119, 563–587. http://dx.doi.org/10.1007/s10546-005-9038-0.

Valentini, R., Matteucci, G., Dolman, A.J., Schulze, E.-D., Rebmann, C., Moors, E.J., Granier, A., Gross, P., Jensen, N.O., Pilegaard, K., Lindroth, A., Grelle, A., Bernhofer, C., Grünwald, T., Aubinet, M., Ceulemans, R., Kowalski, A.S., Vesala, T., Rannik, Ü., Berbigier, P., Loustau, D., Guðmundsson, J., Thorgeirsson, H., Ibrom, A., Morgenstern, K., Clement, R., Moncrieff, J., Montagnani, L., Minerbi, S., Jarvis, P.G., 2000. Respiration as the main determinant of carbon balance in European forests. Nature 404, 861–865. http://dx.doi.org/10.1038/35009084.

Vickers, D., Mahrt, L., 2006. A solution for flux contamination by mesoscale motions with very weak turbulence. Bound.-Layer Meteorol. 118, 431–447.

Villani, M.G., Schmid, H.P., Su, H.-B., Hutton, J.L., Vogel, C.S., 2003. Turbulence statistics measurements in a northern hardwood forest. Bound.-Lay. Meteorol. 108, 343–364. http://dx.doi.org/10.1023/A:1024118808670.